

Impact of stochastic gas motions on galaxy cluster abundance profiles

P. Rebusco ¹, E. Churazov ^{1,2}, H. Böhringer ³, W. Forman ⁴

¹ Max-Planck-Institut für Astrophysik, Karl-Schwarzschild-Strasse 1, 85741 Garching, Germany

² Space Research Institute (IKI), Profsoyuznaya 84/32, Moscow 117810, Russia

³ MPI für Extraterrestrische Physik, P.O. Box 1603, 85740 Garching, Germany

⁴ Harvard-Smithsonian Center for Astrophysics, 60 Garden St., Cambridge, MA 02138, USA

18 February 2019

ABSTRACT

The impact of stochastic gas motions on the metal distribution in cluster core is evaluated. Peaked abundance profiles are a characteristic feature of clusters with cool cores and abundance peaks are likely associated with the brightest cluster galaxies (BCGs) which dwell in cluster cores. The width of the abundance peaks is however significantly broader than the BCG light distribution, suggesting that some gas motions are transporting metals originating from within the BCG. Assuming that this process can be treated as diffusive and using the brightest X-ray cluster A426 (Perseus) as an example, we estimate that a diffusion coefficient of the order of $2 \cdot 10^{29} \text{ cm}^2 \text{ s}^{-1}$ is needed to explain the width of the observed abundance profiles. Much lower (higher) diffusion coefficients would result in too peaked (too shallow) profiles. Such diffusion could be produced by stochastic gas motions and our analysis provides constraints on the product of their characteristic velocity and their spatial coherence scale. We speculate that the activity of the supermassive black hole of the BCG is driving the stochastic gas motions in cluster cores. When combined with the assumption that the dissipation of the same motions is a key gas heating mechanism, one can estimate both the velocity and the spatial scale of such a diffusive processes.

Key words: clusters: individual: Perseus - cooling flows

1 INTRODUCTION

Heavy metals are observed through X-ray spectroscopy of the hot gas in galaxy clusters through the emission lines of highly ionized Ca, Si, S, Fe and other elements. These elements are produced in stars and subsequently injected into the intracluster medium (ICM). On average, the metallicity of the cluster ICM is $\sim 1/3$ of the solar value and it does not seem to vary significantly at least up to a redshift of ~ 1 (e.g. Mushotzky & Loewenstein 1997, Tozzi et al. 2003). This lack of evolution and the relative abundances of the different elements suggest an early enrichment of the ICM by type II supernovae (e.g. Finoguenov et al. 2002). With the high spatial and energy resolution of ASCA, Beppo-Sax, Chandra and XMM-Newton, the radial distribution of metals has been recently mapped for a large sample of nearby clusters (e.g. Fukazawa et al. 2000, Irwin & Bregman 2001, De Grandi & Molendi 2001, Schmidt, Fabian & Sanders 2002, Matsushita et al. 2002, Churazov et al. 2003, De Grandi et al. 2004). Clusters can be divided into two groups, depending on their X-ray properties (Jones & Forman 1984): clusters with cool cores (having a peaked surface brightness profile and a cool core centered at the BCG) and

clusters without cool cores (having more or less a flat surface brightness profile in the core and no clear evidence for a cool region near the center). These two groups are traditionally called cooling flow and non-cooling flow clusters (Fabian 1994). The spatial distribution of metals for these two groups is also markedly different: clusters without cool cores have a more or less uniform distribution, while clusters with cool core have strongly peaked abundance profiles (sometimes exceeding the solar abundance) centered at the BCG (e.g. Fukazawa et al. 1994, 2000, Matsumoto et al. 1996, De Grandi & Molendi 2001). Moreover the relative abundances of different elements in the central peaks of cool core clusters suggests that type Ia supernovae have played a significant role in the enrichment process (e.g. Finoguenov et al. 2002, see also Renzini et al. 1993). It is very likely (e.g. Böhringer et al. 2004, De Grandi et al. 2004) that these central abundance peaks are produced predominantly by the stars of the brightest cluster galaxy after the cluster was assembled. If so, then the distribution of the metals should reflect the distribution of the stars (i.e. light) of the BCG and the differences in the light and metal distributions can be used as a proxy for processes which transport and mix

the metals of the ICM. Indeed in the best studied cases such as M87, Centaurus or Perseus (Matsushita et al. 2003, 2004, Churazov et al. 2003) the metal distribution in the central abundance peaks is broader than the BCG light distribution, implying that injected metals diffuse to larger radii.

Another characteristic property of cool core clusters is a short gas cooling time – a factor of 10 to 100 shorter than the Hubble time. Recent X-ray observations (e.g. Peterson et al. 2003, Matsushita et al. 2002, Kaastra et al. 2004) however suggest that the gas does not cool below temperatures of 1-3 keV and an external source of energy is needed to compensate for the gas cooling losses. A number of potential sources of energy have been considered - among them thermal conduction (e.g. Narayan & Medvedev 2001, Voigt & Fabian 2004) or gas motions of different origin. One of the latter family of models utilizes outflows of relativistic plasma, driven by the central super massive black hole (AGN), which interact with the ICM (e.g. Churazov et al. 2001, 2002). The details of the outflow/gas interactions are not yet understood completely and the assumptions on the character of the induced gas motion vary from being almost pure radial (e.g. Fabian et al. 2003) to mostly stochastic (e.g. Churazov et al. 2002). The observed peaked abundance profiles provide a possibility to evaluate the velocities and the spatial scales of these motions. The same motions may affect the thermal balance of the gas in the core by viscous dissipation or by turbulent transport of heat from larger radii (Cho et al., 2003, Kim & Narayan 2003, Voight & Fabian 2004). The relative importance of both mechanisms is compared in Dennis & Chandran (2004).

In this paper we focus on the impact of stochastic gas motions of arbitrary origin on the transport of metals from the BCG through the ICM in cool core clusters. We adopt here a simple assumption that a diffusion approximation can crudely characterize this transport process. Using the brightest X-ray cluster, Perseus (A426), as an example we estimate parameters of the stochastic motions which are broadly consistent with the data.

The structure of the paper is the following. In section 2 the basic input data and the ingredients of the model are described. In section 3 the evolution of the abundance profiles is analyzed for various assumptions on the diffusion coefficient. The results are discussed in section 4. The last section summarizes our findings.

Throughout the paper $H_0 = 70 \text{ km s}^{-1} \text{ Mpc}^{-1}$ is used.

2 THE MODEL

In this section the basic input parameters of the model are described.

2.1 A426 density, temperature and abundance profiles

The electron density n_e and the temperature T_e profiles used here are based on the deprojected XMM-Newton data (Churazov et al. 2003, 2004) which are also in broad agreement with the ASCA (Allen & Fabian 1998), Beppo-Sax (De Grandi & Molendi 2001, 2002) and Chandra (Schmidt et al.

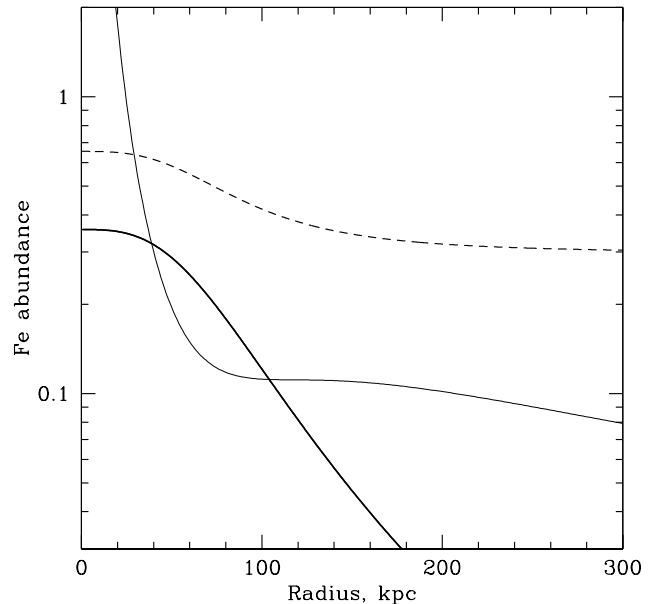


Figure 1. Comparison of the observed and the expected iron abundance profiles for the Perseus cluster. The dashed line shows the observed abundance profile. The adopted profile ignores the central abundance decrement observed in several cooling flow clusters. The thick solid line shows the same profile where a constant value of ~ 0.3 is subtracted. We assume below that this central abundance excess (thick solid line) is primarily due to the metal ejection of the central galaxy. For comparison we show the expected iron abundance (thin solid line) due to the ejection of metals from the galaxies, assuming a SNIa rate of 0.35 SNU, $k = 1.4$ (see the text for definitions) and a cluster age of 8 Gyr. The expected profile was calculated assuming that the ejected metal distribution follows the optical light. The expected abundance profile is much more peaked than the observed profile (due to the contribution of the central galaxy) suggesting that some mechanism is needed to spread the metals.

2002, Sanders et al. 2004) data. Namely:

$$n_e = \frac{4.6 \times 10^{-2}}{[1 + (\frac{r}{57})^2]^{1.8}} + \frac{4.8 \times 10^{-3}}{[1 + (\frac{r}{200})^2]^{0.87}} \text{ cm}^{-3} \quad (1)$$

and

$$T_e = 7 \frac{[1 + (\frac{r}{71})^3]}{[2.3 + (\frac{r}{71})^3]} \text{ keV}, \quad (2)$$

where r is measured in kpc. The hydrogen number density is assumed to be related to the electron number density as $n_H = n_e/1.2$.

For the abundance profile $a(r)$ (Fig.1) we use the deprojected profile obtained from XMM-Newton data (Churazov et al. 2003). The normalization was reduced by 15% percent to match better the most recent deep Chandra observations of the Perseus core (Schmidt et al. 2002, Sanders et al. 2004). Namely:

$$a(r) = 0.3 \frac{2.2 + (r/80)^3}{1 + (r/80)^3} a_{\odot}, \quad (3)$$

where r is in kpc, and a_{\odot} is the solar abundance (Anders

& Grevesse 1989). The functional form used neglects completely the central “abundance hole” observed in the Perseus cluster (Schmidt et al. 2002, Churazov et al. 2003, Sanders et al. 2004) or in M87 (Böhringer et al. 2001, Matsushita, Finoguenov & Böhringer, 2003). The nature of the abundance hole is unclear and it might be related to “visual” effects (like the presence of a nonthermal component in the X-ray continuum emission or resonant scattering, see however Churazov et al. 2004, Gastaldello & Molendi, 2004 for arguments against resonant scattering) rather than to a real decrease of the metal abundance in the very core. The solid line in (Fig.1) is the iron abundance profile from which a constant value of ~ 0.3 was subtracted. We assume below that the central abundance excess is primarily due to the metal ejection from the central galaxy. The total iron mass in the central excess is of the order of $1.3 \cdot 10^9 M_\odot$ (or $\sim 5 \cdot 10^8 M_\odot$ within the central 100 kpc). Compared to Böhringer et al. (2004) the lower overall abundance normalization and the larger value of the subtracted constant lead to somewhat lower masses attributed to the excess.

For comparison we show in Fig.1 the expected iron abundance (thin solid line) due to the ejection of metals from the galaxies, assuming a SNIa rate of 0.35 SNU, $k = 1.4$ (see Section 2.3 for definitions) and a cluster age of 8 Gyr. The expected profile was calculated assuming that the ejected metal distribution follows the optical light. The expected abundance profile is much more peaked than the observed profile (due to the contribution of the central galaxy) suggesting that some mechanism is needed to spread the metals.

2.2 The central galaxy: NGC 1275

The light distribution of the central elliptical galaxy is described here by a simple Hernquist profile (Hernquist 1990). The effective radius $r_e = 15.3$ kpc and the total blue luminosity $2.8 \cdot 10^{11} L_\odot$ are taken from Schombert (1987, 1988). While the actual light profile of NGC1275 is more complicated than a single Hernquist profile, this is an acceptable approximation for the purpose of this study. In Fig.2 the light distribution of the central galaxy is compared with the light distribution of all the other galaxies. The central galaxy dominates up to a distance of ~ 100 kpc.

2.3 Iron and gas injection rates

The bulk of the cluster gas is enriched at early times of cluster formation by a large number of type II supernovae. The central abundance excess is believed to be formed at later times and the main contributors are likely to be the type Ia supernovae and the stellar mass loss associated with the central galaxy (Matsushita et al. 2003, Böhringer et al. 2004, De Grandi et al. 2004). We use here similar iron injection rates as in Böhringer et al. (2004):

$$\left(\frac{dM_{Fe}}{dt} \right)_{SNIa} = SR \cdot 10^{-12} \left(\frac{L_B}{L_\odot^B} \right) \eta_{Fe} \quad (4)$$

$$= R(t) \cdot 0.105 \times 10^{-12} \left(\frac{L_B}{L_\odot^B} \right) M_\odot \text{ yr}^{-1},$$

$$\left(\frac{dM_{Fe}}{dt} \right)_* = \gamma_{Fe} \cdot 2.5 \cdot 10^{-11} \left(\frac{t}{t_H} \right)^{-1.3} \quad (5)$$

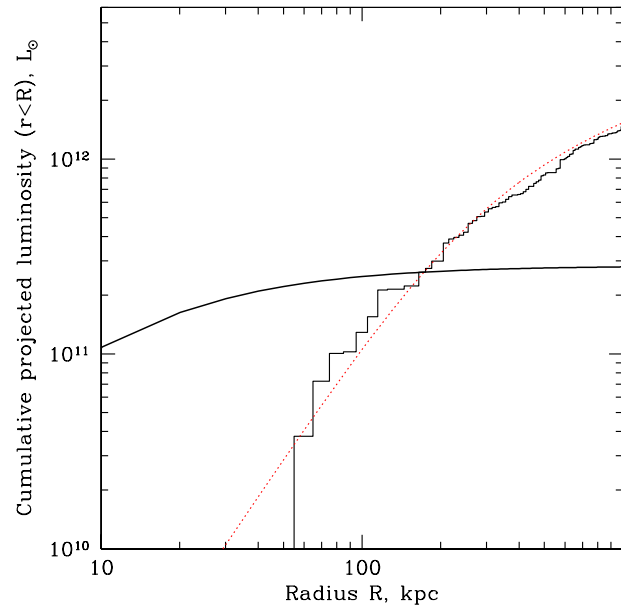


Figure 2. Cumulative projected light distribution of the central galaxy NGC1275 (thick solid line) and of the other galaxies (histogram). The positions and the magnitudes of the galaxies are taken from Brunzendorf & Meusinger (1999). A simple King model fit to the light distribution (omitting NGC1275) is shown. The central galaxy dominates light up to a distance of ~ 100 kpc.

$$\times \left(\frac{L_B}{L_\odot^B} \right) M_\odot \text{ yr}^{-1},$$

where SR is the present SNIa rate in SNU, $\eta_{Fe} = 0.7 M_\odot$ is the iron yield per SNIa, $\gamma_{Fe} = 2.8 \cdot 10^{-3}$ is the mean iron mass fraction in the stellar winds of an evolved stellar population, t_H is the Hubble time. The expression for the stellar mass loss was adopted from Ciotti et al. (1991), assuming a galactic age of 10 Gyr. The gas injection (not only iron) due to stellar mass loss is important only in the central ~ 20 kpc and it was neglected in the subsequent calculations. The time dependent factor $R(t) = (t/t_H)^{(-k)}$ takes into account an increased SNIa rate in the past (Renzini et al. 1993), with the index k ranging from 1.1 up to 2. A fiducial value for the SNIa rate of 0.15 SNU (Cappellaro, Evans, & Turatto 1999) was assumed. Thus the total iron injection rate within a given radius r can be written as

$$s(< r, t) = \left(\frac{dM_{Fe}}{dt} \right)_* + \left(\frac{dM_{Fe}}{dt} \right)_{SN} \propto \left(\frac{L_B(< r)}{L_\odot^B} \right) \quad (6)$$

The total amount of iron produced by the central galaxy during its evolution from some initial time to the present is simply an integral of equation (6) over time. The total amount of iron in the central excess is set above (by our definition of the central excess, see Fig.1) to $\sim 1.3 \cdot 10^9 M_\odot$. Therefore, the parameters of the model (SR , k , t_{age}) are constrained by the observed total iron mass (see Fig.3).

For the subsequent analysis we have selected two combinations of these parameters: (0.35, 1.4, 8 Gyr) and (0.26, 2, 8 Gyr). With these choices of parameters one can read-

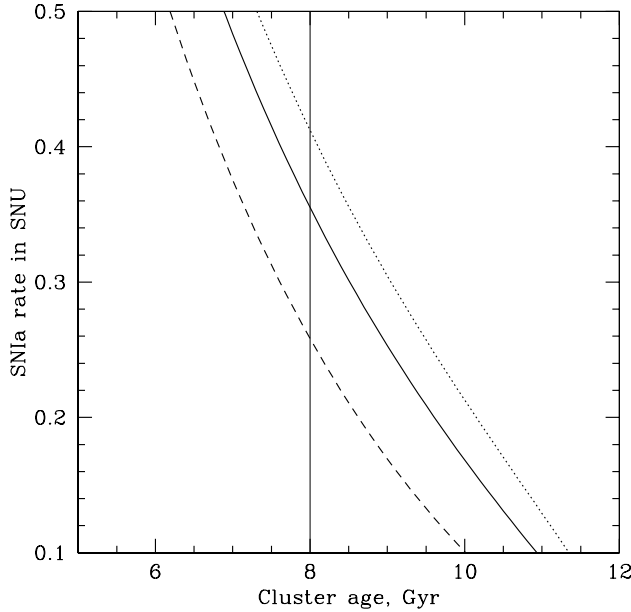


Figure 3. SNIa rate in SNU required to produce the excess amount of iron of $\sim 1.3 \cdot 10^9 M_\odot$ by the BCG with $L_B = 2.8 \cdot 10^{11} L_\odot$ according to eq.6. The solid line is for $k = 1.4$, the dotted one for $k = 1.1$, the dashed one for $k = 2$

ily predict the amount and the distribution of the metals ejected from the galaxies into the ICM as displayed in Fig.1. In this figure we show the observed iron abundance and the expected iron abundance, determined by comparing the amount of injected iron (by all the galaxies, including the BCG) with the present day gas density distribution. On large scales $\sim 30\%$ of the observed amount of iron is provided by SNIa and stellar mass loss. The remaining $\sim 70\%$ could be attributed to early enrichment by SNII. The central excess of iron generated by the central galaxy is much more peaked than the observed abundance profile. This is of course an expected result, given that the effective radius of the galaxy is ~ 15 kpc, while the characteristic size of the abundance excess is much larger. The difference between the distribution of the ejected iron and the observed abundance profile suggests that some process is transporting the metals to larger radii. We assume below that this process can be treated in a diffusion approximation.

2.4 Diffusion of metals due to stochastic gas motions

We assume that the ICM at a given radius r is involved in stochastic motions with a characteristic size sufficiently smaller than r and that this motion mixes the ICM. We assume moreover that such motion with a characteristic velocity v and a characteristic coherence length l will lead to an effective diffusion coefficient of the order of $D \sim \frac{vl}{3}$. We further make the strong simplification that the gas density and temperature do not evolve with time, i.e. the gas entropy losses (due to radiation) and gains (due to the dissipation of the stochastic motions and to the mixing of the low entropy

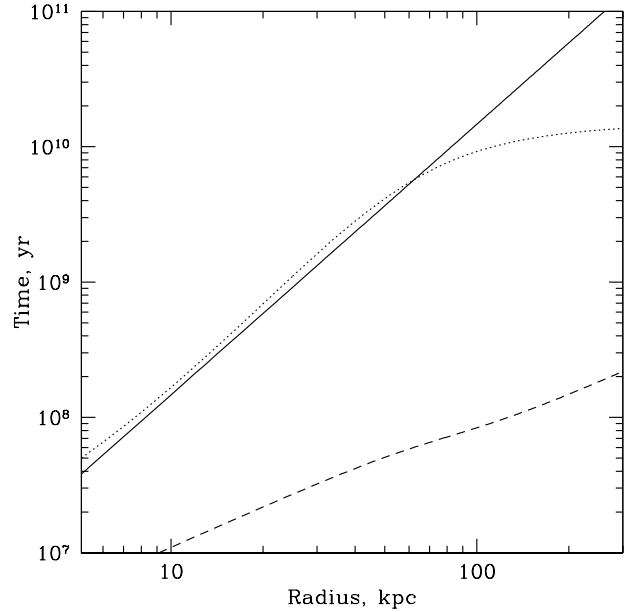


Figure 4. Diffusion time scale (solid line) estimated as $t_{\text{diff}} \sim r^2/D$, where $D = 2 \cdot 10^{29} \text{ cm}^2 \text{ s}^{-1}$. For comparison the cumulative enrichment time (ratio of the amount of metals in the abundance excess to the metal ejection rate by the central galaxy) is shown by the dotted line. The dashed line shows the sound crossing time.

gas with the outer layers of higher entropy gas) cancel each other. In this approximation the stochastic motions have a clear impact on the distribution of metals and this process can be considered in a diffusion approximation:

$$\frac{\partial na}{\partial t} = \nabla \cdot (D \nabla na) + S, \quad (7)$$

where $n = n(r)$ is the gas density, $a = a(r, t)$ is the iron abundance and $S = S(r, t)$ is the source term due to the iron injection from the central galaxy, D is the diffusion coefficient. Once the diffusion coefficient is specified, eq.7 can be readily integrated.

A rough estimate of the required diffusion coefficient can be obtained by comparing the characteristic time scales for diffusion and enrichment (Fig.4). In this figure the cumulative iron enrichment time - i.e. the ratio of the observed amount of metals in the abundance excess within a given radius r is compared to the current injection rate of iron by the central galaxy within the same radius. The diffusion time was estimated as $t_{\text{diff}} \sim r^2/D$, where the diffusion coefficient D is set to $2 \cdot 10^{29} \text{ cm}^2 \text{ s}^{-1}$. Fig.4 suggests that diffusion with coefficient $D \sim 2 \cdot 10^{29} \text{ cm}^2 \text{ s}^{-1}$ would significantly affect the metal distribution in the core.

3 RESULTS

3.1 Constant diffusion coefficient

In a more detailed modeling of the diffusion transport of metals in the ICM, we first consider the simplest case of a diffusion coefficient which is independent of both time

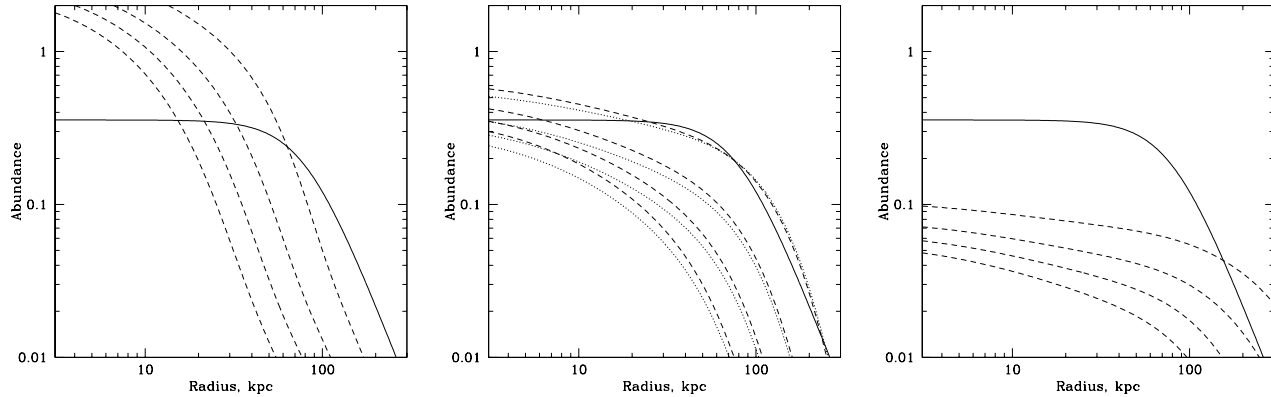


Figure 5. Time evolution of the abundance profiles for different diffusion coefficients $D = 2 \cdot 10^{28}, 2 \cdot 10^{29}, 2 \cdot 10^{30} \text{ cm}^2 \text{ s}^{-1}$ for the left, middle and right plots respectively. The thick solid line is the observed abundance peak, while the dashed lines show the abundance of metals produced by the central galaxy during 1,2,4 and 8 Gyr (from the bottom to the top) in the model with $k = 1.4$ and $SR = 0.35$. For comparison in the middle plot the dotted line shows the same evolution for $k = 2$ and $SR = 0.26$.

and radius. Fig.5 shows the evolution of the abundance peak produced by the central galaxy after 1, 2, 4 and 8 Gyr for different values of the diffusion coefficient: $D = 2 \cdot 10^{28}, 2 \cdot 10^{29}, 2 \cdot 10^{30} \text{ cm}^2 \text{ s}^{-1}$ for the left, middle and right plots respectively. The thick line in all plots shows the observed abundance peak. It is clear that too small (or too large) diffusion coefficients produce too peaked (or too shallow) abundance profiles, while $D = 2 \cdot 10^{29} \text{ cm}^2 \text{ s}^{-1}$ is roughly consistent with the data. These calculations were done assuming $k = 1.4$ and $SR = 0.35$. The comparison with the alternative model with $k = 2$ and $SR = 0.26$ (dotted curves in the middle plot) shows that the differences in the shape of the final abundance excess are minor.

A similar characteristic value of the diffusion coefficient can be derived by comparing the characteristic size of the observed abundance excess and the excesses produced by ejection and diffusion in the model. Fig.6 shows the effective radius (the radius containing half of the ejected metals) as a function of the diffusion coefficient. For small diffusion coefficients the metal distribution is essentially set by the light distribution of the central galaxy. As the diffusion coefficient increases the effective radius also increases. This plot also suggests that $D \sim 2 \cdot 10^{29} \text{ cm}^2 \text{ s}^{-1}$ would provide a width of the metal distribution similar to the one observed in the abundance excess. One can further consider the present day evolution of the abundance profile, i.e. using the observed abundance peak as an initial condition, as shown in Fig.7. Again, too small (or too large) diffusion coefficients cause a quick steepening or flattening of the abundance peaks on time scales of Gyr. The evolution of the profile for the diffusion coefficient of the order of $2 \cdot 10^{29} \text{ cm}^2 \text{ s}^{-1}$ is much more gradual.

3.2 Varying diffusion coefficient as a function of radius

In this section we estimate the impact of diffusion on the abundance peaks when the diffusion coefficient is a function of the radius. One natural motivation for such an assumption is the hypothesis that an AGN at the center of the BCG

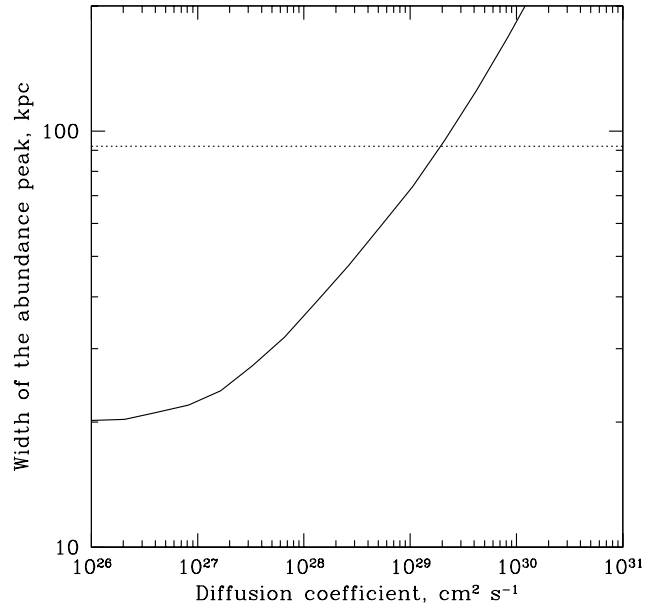


Figure 6. Width of the abundance peak distribution (radius containing half of the ejected iron) as a function of the diffusion coefficient for $k = 1.4$ and 8 Gyr cluster age. The dotted horizontal line shows the width of the observed abundance excess.

is driving the gas motions in the core. In this case one would expect these motions to fade away outside the cluster core, when the energy injected by the AGN into the ICM spreads over large masses of gas. Let us assume that a fraction f of the ICM volume at a given radius is involved in the stochastic motions with characteristic velocity v and spatial scale l . If the dissipation of the stochastic motions with the rate $\Gamma_{diss} \propto nv^3/l$ is the main source of energy which offsets the gas radiative losses $\Gamma_{cool} \propto n^2\Lambda(T)$, then $f\Gamma_{diss} \sim \Gamma_{cool}$ and therefore $f \propto n$ (if l and v do not vary strongly with

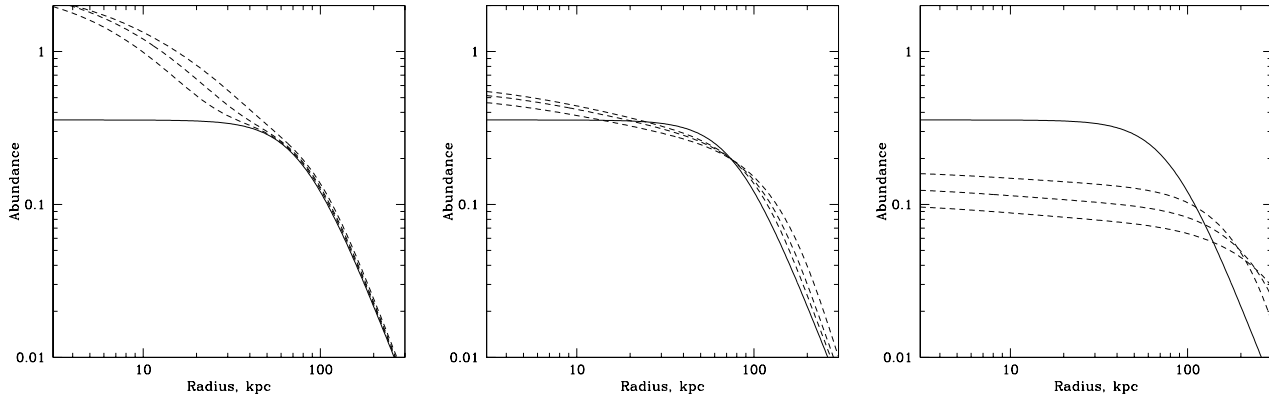


Figure 7. Time evolution of the abundance profiles starting from the observed abundance peak for different diffusion coefficients: $D = 2 \cdot 10^{28}, 2 \cdot 10^{29}, 2 \cdot 10^{30} \text{ cm}^2 \text{ s}^{-1}$ for the left, middle and right plots respectively. The initial profile is the observed abundance peak distribution and the evolution of the profile is shown after 1,2 and 4 Gyr (dashed curves from the bottom to the top) for the model with $k = 1.4$ and $SR = 0.36$. The thick solid line is the observed abundance peak. The calculations were done assuming metal injection rates according to eq.6, starting from $t = t_H$. Note that for the figures on the left(right) the profile quickly evolves to a peaked (shallow) distribution, while for the central plot ($D = 2 \cdot 10^{29} \text{ cm}^2 \text{ s}^{-1}$) the evolution is very slow, approximately corresponding to a quasi-steady state.

the radius). The effective diffusion coefficient can then be written as $D \propto n$, i.e. D declines with the radius along with the density. This is of course an oversimplified scaling, but to see the influence of the diffusion coefficient changing with radius on the abundance profile, we parametrized it as $D = D_0 (n(r)/(n(r_0)))^\alpha$, where $D_0 = 2 \cdot 10^{29} \text{ cm}^2 \text{ s}^{-1}$, $r_0 = 50 \text{ kpc}$. The resulting profiles for $\alpha = 1, 2, -1$ are shown in Fig.8. For declining diffusion coefficients, for larger values of α , the overall shape of the peak becomes more boxy than for a constant diffusion coefficient (see Fig.5 middle panel). In fact the profile with $\alpha = 1$ is closer to the observed abundance peak than that with a constant diffusion coefficient. However, given the uncertainties of the adopted abundance peak and the oversimplified nature of the model, one cannot claim that a variable diffusion coefficient provides a significantly better description of the observed abundance peak.

The right plot in Fig.8 is calculated for $\alpha = -1$, i.e. diffusion coefficient rising with the radius (or with a decline of the density). This case represents the situation when the gas in the very center is more steady than in the outer layers. With our choice of D_0 and scaling radius r_0 the predicted profiles are too peaked compared to that observed. Of course with such simulations we cannot constrain the behavior of the diffusion coefficient at even larger radii where the stochastic motions produced by e.g. mergers may stir and mix the ICM. We can only conclude that within the core of the cluster diffusion coefficients declining with radius seem preferable compared to rising ones.

4 DISCUSSION

4.1 Constraints on the velocities and spatial scales

Summarizing the results of the above section we conclude that the shape of the observed abundance peak produced by metal ejection from the central galaxy is consistent with the presence of a diffusive transport of iron with effective dif-

fusion coefficient of the order of $D_0 \sim 2 \cdot 10^{29} \text{ cm}^2 \text{ s}^{-1}$. Under the assumption that the diffusion of iron is due to stochastic gas motions on much smaller spatial scales (smaller than the radius r), one can express the diffusion coefficient in the form $D \sim C_1 v l$, where C_1 is a dimensionless constant of the order of unity. Thus the value of D_0 estimated in the previous section can be considered as a measure of the product of the characteristic velocity v and the spatial scale l of the gas motions. On the other hand the gas heating rate due to the dissipation of the kinetic energy of the same motions also depends on the combination of v and l and can be written as $\Gamma_{diss} \sim C_2 \rho v^3 / l$, where ρ is the gas density and C_2 is a dimensionless constant. Assuming that the dissipation of turbulent motions is the dominant source of heat and that the heating rate is equal to the gas cooling rate then $\Gamma_{diss} \sim \Gamma_{cool} = n^2 \Lambda(T)$. The cooling rate can be easily calculated from the observed gas temperature and density, thus providing another constraint on v and l . Therefore using D_0 and the cooling rate, one can estimate both v and l . The coefficients C_1 and C_2 (and the validity of the scaling itself) in the above expressions depend critically on the character of the gas motions, which is unknown. One can hope to derive an order of magnitude estimate using the simplest variants of turbulent flows. For this estimate we follow the definitions of Dennis & Chandran (2004) for v and l which lead to the following expressions for D and Γ_{diss} :

$$D \sim 0.11 v l \quad (8)$$

$$\Gamma_{diss} \sim 0.4 \rho v^3 / l. \quad (9)$$

Using the above definitions and choosing $r = 50 \text{ kpc}$ as a characteristic radius we set $D = 2 \cdot 10^{29} \text{ cm}^2 \text{ s}^{-1}$ and $\Gamma_{diss} = n^2 \Lambda(T)$ to balance cooling and dissipation. One can plot the resulting constraints in a v/l plot (see Fig.9). The thick solid line shows the combinations of v and l which give the same diffusion coefficient, while along the thick dotted line the dissipation rate is equal to the cooling rate at $r = 50 \text{ kpc}$. The two pairs of solid and dotted lines show the effect

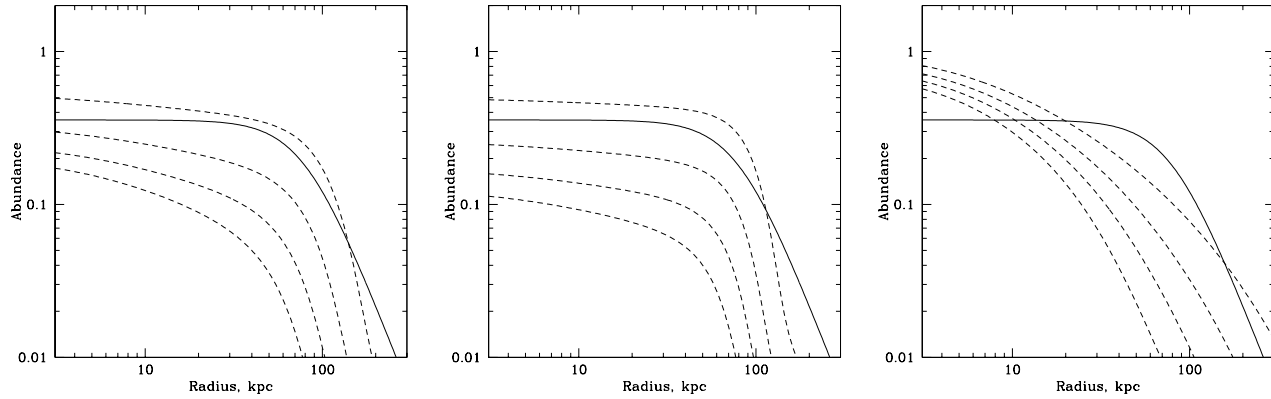


Figure 8. Time evolution of the abundance profiles for different radial dependence of the diffusion coefficient parametrized as $D = D_0 (n(r)/(n(r_0)))^\alpha$. $\alpha = 1, 2, -1$ for the left, middle and right plots respectively. $D_0 = 2 \cdot 10^{29} \text{ cm}^2 \text{ s}^{-1}$, n is the gas density, $r_0 = 50 \text{ kpc}$. The thick solid line is the observed abundance peak, while the dashed lines show the abundance of metals produced by the central galaxy during 1, 2, 4 and 8 Gyr (in the model with $k = 1.4$ and $SR = 0.35$). As α increases the distribution becomes more boxy, while for negative α the distribution is more steep than the observed one.

of varying C_1 and C_2 by factor of 1/3 and 3 each. The intersection of the two curves (bands) gives the locus of the combinations of l and v such that on one hand the diffusion coefficient is approximately equal to D_0 and on the other hand the dissipation rate is approximately equal to the cooling rate. In this figure l and v are the characteristic spatial scales and velocities of the stochastic gas motions (see Dennis & Chandran 2004 and references therein). This simplified model suggests that eddies with size of $\sim 10 \text{ kpc}$ and velocities of the order of few hundred km/s can provide the appropriate iron diffusion and balance gas cooling losses at the same time. Such velocities and spatial scales seem reasonable for models where AGN driven outflows are present in cool cluster cores. In these models the outflow generates motions of the gas on spatial scales of expanding and rising bubbles (10-15 kpc for the case of A426) and with velocities characteristic for outflows (a fraction of the sound speed or few hundred km/s for buoyantly rising bubbles). These gas motions eventually dissipate their energy through viscous heating and/or shocks. The latter mechanism of dissipation could occur almost without any mixing of metals - if e.g. there are predominantly radial shock waves, while the former mechanism provides a closer link between heating and metal diffusion. While the estimates from Fig.9 are very crude, they are consistent with the assumption that the mixing/dissipation process plays an important role in clusters with cool cores. The presence of differential motions with velocities of the order of few hundred km/s is also consistent with the lack of spectral signatures of resonant scattering in the Perseus cluster (Churazov et al. 2004), although resonant scattering is sensitive to both isotropic (case with mixing of metals) and radial (no mixing) gas motions.

We stress again that the uncertainties in the expressions for the turbulent diffusion coefficient and for the dissipation rate (see eqns.8-9) are very large and that the numerical results (Fig.9) should be treated with caution. Moreover the actual transport of metals in a stratified cluster medium could be very complicated (e.g. Brueggen 2002), involving on one hand stages of efficient transport of metals entrained

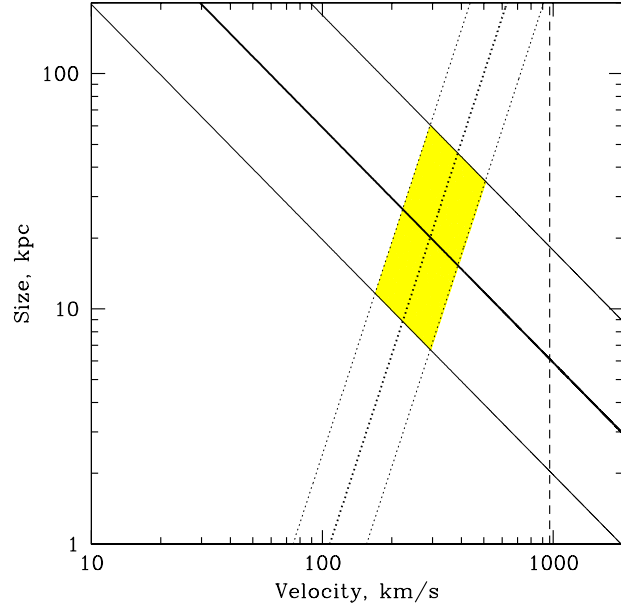


Figure 9. Constraints on the characteristic velocity and spatial size. The thick solid line corresponds to $D = 2 \cdot 10^{29} \text{ cm}^2 \text{ s}^{-1}$. The thick dotted line corresponds to $\Gamma_{diss} = n^2 \Lambda(T)$. To the left of this line, cooling dominates over heating by dissipation. At intersection of these curves, $v \sim 300 \text{ km s}^{-1}$ and $l \sim 20 \text{ kpc}$, gas cooling is balanced by the dissipation and the diffusion coefficient is of the right order. The thin solid and the dotted lines correspond to a variation of the coefficients in eqns. 8 - 9 by factors of 0.3 and 3. The vertical dashed line shows the sound velocity in the gas.

with the rising bubbles and on the other hand separation of the enriched clumps from the rising flow due to the entropy contrast. However the above analysis suggests that cool cores could be a long lived feature (at least few Gyr - judging from the amount of metals ejected by the BCG - see Böhringer

et al. 2004, De Grandi et al. 2004), supported against the catastrophic cooling by the AGN activity.

Of course AGN activity is not the only mechanism which can induce motions in the cluster core. The evidence for gas “sloshing” (Markevitch, Vikhlinin & Forman, 2003) is found in more than 2/3 of the cooling flow clusters and both mergers or AGN activity may be the cause. Fujita, Matsumoto & Wada (2004) argue that the turbulence in the core is caused by the bulk gas motions of the cluster gas. Depending on the characteristic spatial and velocity scales of the motions either direct dissipation or turbulent heat transport may affect the thermal state of the gas (Dennis & Chandran, 2004).

4.2 Alternative scenarios for the abundance peak formation.

The ejection of metals from the central BCG is not the only mechanism which could contribute to the formation of abundance peaks in cool core clusters. Given the uncertainties in the age of the system and in the rate of metal ejection by stars, one cannot exclude other sources of iron based on a simple comparison of the excess iron mass with the optical luminosity of the central galaxy. We briefly mention below the most obvious alternative channels of metal enrichment.

One of the processes which could lead to an enhanced abundance of metals in the cluster core is gravitational settling (e.g. Fabian & Pringle 1977, Rephaeli 1978, Gilfanov & Sunyaev 1984, Chuzhoy & Loeb 2004). For the iron this process is very slow and it is unlikely that it plays an important role in modifying the observed peaked iron distributions.

More promising seems to be the stripping of metal enriched gas from smaller subclusters and groups which may have lower entropy than the bulk of the cluster ICM: group/subcluster gas may sink to the bottom of the potential well (e.g. Churazov et al. 2003), unless hydrodynamical instabilities mix it with the ICM before it reaches the cluster center.

In a similar way, stripping the interstellar medium (ISM) of infalling spirals or elliptical galaxies (e.g. Böhringer et al. 1997, Tonizawa & Schindler, 2001) that spend a large part of their time in orbit at large radii can lead to a concentration of metals in the cluster center in comparison to the overall galaxy distribution. A closer inspection of the expected effect of the stripping of the bulk of the ISM from spirals at column densities of $10^{20} - 10^{21} \text{ cm}^{-2}$ shows that this should occur at gas densities less than $n_e \sim 10^{-4} \text{ cm}^{-3}$ for spiral galaxies falling in face on and at somewhat larger densities if the galaxies are inclined but little ISM should reach the inner part of the cluster with gas densities larger than $n_e \sim 10^{-3} \text{ cm}^{-3}$ (e.g. Cayatte et al. 1994, Böhringer et al. 1997). Thus most of the stripping enrichment of the ICM should happen outside a radius of 300 kpc and well outside the region considered here. Stripping should take place both in cooling flow and non-cooling flow clusters. And unless all non-cooling flow clusters have experienced a recent merger one would expect abundance gradients in both types of clusters.

The good correlation of the BCG luminosity and the iron excess mass (e.g. De Grandi et al. 2004) seems to suggest that the above mentioned alternative mechanisms do not play a dominant role in the formation of the cen-

tral abundance excess. Nevertheless it is not easy to discard these mechanisms completely. One can hope that with the launch of ASTRO-E it will be possible to derive new constraints on the character of the gas motions in the cool cores clusters, in particular on the amplitude and the characteristic spatial scales of the velocity perturbations in the cluster cores. The anticipated energy resolution of ASTRO-E spectrometer - FWHM $\sim 6.7 \text{ eV}$ (see e.g. <http://heasarc.gsfc.nasa.gov/docs/astroe>) corresponds to velocities of $\sim 200 \text{ km/s}$ for the 6.7 keV line. For comparison the width of the 6.7 keV line due to thermal motions of iron ions is $\sim 100 \text{ km/s}$ (at a temperature of 3 keV). Therefore it is realistic to expect the detection of line broadening for characteristic stochastic velocities larger than $\sim 100 \text{ km/s}$. The position of the line can be measured with much higher accuracy and therefore the presence of large scale motions can be verified. Given the angular size of a single spectrometer pixel of $\sim 0.5'$, the spatial scales one can probe in Perseus are of order of 10 kpc. Thus Perseus observations with ASTRO-E will provide a decisive test of the models discussed above.

5 CONCLUSIONS

We show that the heavy metal abundance peak observed in the Perseus cluster is consistent with a diffusive spreading of metals, provided that the diffusion coefficient is of the order of $2 \cdot 10^{29} \text{ cm}^2 \text{ s}^{-1}$. Stochastic gas motions with characteristic velocities of the order of few hundred km/s and spatial scales of the order of 10 kpc can provide the diffusive transport of iron and simultaneously a dissipation rate comparable with the gas cooling rate. Such parameters seem to be broadly consistent with models where self-regulated AGN driven outflows are present in the cool cores clusters. ASTRO-E2 observations of Perseus should provide a clear test of the importance of turbulent mixing in cool cluster cores.

REFERENCES

- Allen, S. W., Fabian, A. C., 1998, MNRAS, 297, L63
- Anders E., Grevesse N., 1989, Geochimica et Cosmochimica Acta, 53, 197
- Boehringer H., Neumann D. M., Schindler S., Huchra J. P., 1997, ApJ, 485, 439
- Böhringer H., Belsole, E., Kennea, J., et al. 2001, A&A, 365, L18
- Böhringer H., Matsushita K., Churazov E., Finoguenov A., Ikebe Y., 2004, A&A
- Brüggen, M., 2002, ApJ, 571, L13
- Brunzendorf, J., Meusinger H., 1999, ApJS, 139, 141
- Cappellaro E., Evans R., Turatto M., 1999, A&A, 351, 459
- Cayatte V., Kotanyi C., Balkowski C., van Gorkom J. H., 1994, AJ, 107, 1003
- Cho J., Lazarian A., Honein A., Knaepen B., Kassinos S., Moin P., 2003, ApJ, 589, L77
- Churazov E., Sunyaev R., Forman W., Böhringer H., 2002, MNRAS, 332, 729
- Churazov E., Brüggen M., Kaiser C. R., Böhringer H., Forman W., 2001, ApJ, 554, 261
- Churazov, E., Forman, W., Jones, C., Böringer, H., 2003, ApJ, 590, 225

Churazov, E., Forman, W., Jones, C., Sunyaev, R., Böringer, H.
 2004, MNRAS, 347, 29

Chuzhoy, L., Loeb, A., MNRAS, 349, L13

Ciotti L., D'Ercole A., Pellegrini S., Renzini A., 1991, ApJ 376
 380

De Grandi, S., Ettori, S., Longhetti, M., Molendi, S., 2004, A&A,
 419, 7

De Grandi S., Molendi S., 2001, ApJ, 551, 153

De Grandi S., Molendi S., 2002, ApJ 567 163

Dennis, T., Chandran, B., 2004, ApJ, accepted

Fabian, A.C., Pringle, J.E., 1977, MNRAS, 181, 5

Fabian, A.C. 1994, ARA&A, 32, 277

Fabian A. C., Sanders J. S., Allen S. W., Crawford C. S., Iwasawa
 K., Johnstone R. M., Schmidt R. W., Taylor G. B., 2003,
 MNRAS, 344, L43

Finoguenov A., Matsushita K., Böhringer H., Ikebe Y., Arnaud
 M., 2002, A&A, 381, 21

Fukazawa Y., Ohashi T., Fabian A. C., Canizares C. R., Ikebe Y.,
 Makishima K., Mushotzky R. F., Yamashita K., 1994, PASJ,
 46, L55

Fukazawa Y., Makishima K., Tamura T., Nakazawa K., Ezawa
 H., Ikebe Y., Kikuchi K., Ohashi T., 2000, MNRAS, 313, 21

Gilfanov, M.R., Sunyaev, R.A., 1984, SvAL, 10, 137

Gastaldello, F., Molendi, S., 2004, ApJ, 600, 670

Hernquist L., 1990, ApJ, 356, 359

Irwin J. A., Bregman J. N., 2001, ApJ, 546, 150

Jones C., Forman W., 1984, ApJ, 276, 38

Kaastra J. S., et al. 2004, A&A, 413, 415

Kim, W., Narayan, R. 2003, ApJ, 596L, 139

Markevitch M., Vikhlinin A., Forman W. R., Matter and En-
 ergy in Clusters of Galaxies, ASP Conference Proceedings,
 Vol. 301. Held 23-27 April 2002 at National Central Univer-
 sity, Chung-Li, Taiwan. Edited by Stuart Bowyer and Chorng-
 Yuan Hwang. San Francisco: Astronomical Society of the Pa-
 cific, 2003. ISBN: 1-58381-149-4, p.37

Matsumoto H., Koyama K., Awaki H., Tomida H., Tsuru T.,
 Mushotzky R., Hatsukade I., 1996, PASJ, 48, 201

Matsushita, K., Belsole, E., Finoguenov, A., Böhringer, H., 2002,
 A&A, 386, 77

Matsushita, K., Finoguenov, A., Böhringer, H., 2003, A&A, 401,
 443

Matsushita, K., Böhringer, H., Takahashi, I., Ikebe, Y., 2004,
 A&A, in press

Mushotzky, R. F., Loewenstein, M., 1997, ApJ, 481, L63

Narayan R., Medvedev M. V., 2001, ApJ, 562, L129

Peterson J. R., Kahn S. M., Paerels F. B. S., Kaastra J. S.,
 Tamura T., Bleeker J. A. M., Ferrigno C., Jernigan J. G.,
 2003, ApJ, 590, 207

Renzini A., Ciotti L., D'Ercole A., Pellegrini S., 1993, ApJ, 419,
 52

Rephaeli, Y., 1978, ApJ, 225, 335

Sanders J. S., Fabian A. C., Allen S. W., Schmidt R. W., 2004,
 MNRAS, 349, 952

Schmidt, R.W., Fabian, A.C., Sanders, J.S., 2002, MNRAS, 337,
 71

Schombert J. M., 1987, ApJSS, 64, 643

Schombert J. M., 1988, ApJ 328 475

Tonizawa T., Schindler S., 2001, MNRAS, 325, 509

Tozzi P., Rosati P., Ettori S., Borgani S., Mainieri V., Norman
 C. 2003, ApJ, 593, 705

Voigt L. M., Fabian A. C. 2004, MNRAS, 347, 1130